

# Generation and Measurement of High Intermittent Heat Flux in GAMMA 10/PDX<sup>\*)</sup>

Ryutaro MINAMI, Tsuyoshi KARIYA, Tsuyoshi IMAI, Tomoharu NUMAKURA, Maki OKADA, Toshitaka HOJO, Fumiya MOTOYOSHI, Takuya YABUSA, Nao HIMENO, Yoichi ENDO and Yousuke NAKASHIMA

*Plasma Research Center, University of Tsukuba, Tsukuba, Ibaraki 305-8577, Japan*

(Received 29 September 2018 / Accepted 18 December 2018)

Electron cyclotron heating (ECH) power modulation experiments have been conducted for GAMMA 10/PDX to generate and control the high heat flux and to develop an edge localized mode (ELM)-like intermittent heat load pattern for divertor simulation studies. Flux and energy spectra of end-loss electrons are measured using a multi-grid energy analyzer (loss electron diagnostics, LED). ECH-induced potential formation at plug regions (P-ECH) produces high-energy electron flows along the magnetic lines of force. The power scaling of electron flux in GAMMA 10/PDX indicates that higher ECH power generates higher electron flux. In this study, a new mirror antenna is developed to generate higher heat flux and concentrate the heating power on the axis. The energy density and heat flux obtained using previous systems are  $0.06 \text{ MJ/m}^2$  and  $11.4 \text{ MW/m}^2$ , respectively, and those obtained using the new mirror systems are  $0.09 \text{ MJ/m}^2$  and  $30 \text{ MW/m}^2$ , respectively. These values are still considerably lower than those of ITER ELM (mitigated ELMs in ITER is  $\sim 0.5 \text{ MJ/m}^2$  for  $t = 0.5 \text{ ms}$ ).

© 2019 The Japan Society of Plasma Science and Nuclear Fusion Research

Keywords: ECH power modulation, high heat flux, ELM, gyrotron, GAMMA 10/PDX

DOI: 10.1585/pfr.14.2402034

## 1. Introduction

Boundary plasma physics is essential for sustaining a steady-state fusion reactor plasma. Controlling divertor plasma and understanding the physics of plasma-wall interactions are the fundamental issues related to ITER and fusion research. The GAMMA 10/PDX project aims to develop mirror devices for fusion-reactor-based studies, including potential control and end losses, transport of particles and heat fluxes, and the physics of divertor plasma and plasma-wall interaction. The divertor plasma simulator, known as E-Divertor, uses the high heat flux generated at the open end of the GAMMA 10.

The most practical application of the GAMMA 10 mirror plasma for divertor simulations uses the axial loss as the particle and heat flux simulator [1]. Edge localized mode (ELM) characterizations have provided important insights into the high heat load divertor simulator experiments. Modulating the fundamental electron cyclotron heating (ECH) at the plug region (P-ECH) produces arbitrary pulse heat load patterns. The ELM intermittent heat pulses can be simulated by changing the on/off timing. One pulse heat load energy density depends on the ECH power.

P-ECH has been previously employed to form a plasma-confining (plug) potential in the axi-symmetric mirror cell at either machine ends. This system has been studied in relation to potential formation at the plug re-

gion. The fundamental ECH produces a substantial axial flux of warm electrons and its production mechanism considerably affects potential formation. Thus, the experimental analyses of the warm electron flux will provide insights into the heating process and potential formation.

A multi-grid-type electrostatic energy analyzer is often employed to interpret the end-loss physics of a given system for end-loss-electron observations. Multi-grid-type electrostatic analyzers have been widely used to measure the end-loss particles from a mirror machine because the electrons flow into an end region along the magnetic lines of force. In this study, accelerated electrons at a machine end are directly detected using the open field configuration of GAMMA 10 and by examining the effects of ECH on the electrons.

Recently, a 28 GHz gyrotron that could achieve  $>1.5 \text{ MW}$  for GAMMA 10 and other low B field device ECH sources has been developed. Using multi-MW and multi-frequency technologies for robust and cost effective reactor heating systems is a major challenge. GAMMA 10/PDX project primarily focuses on developing a high-power 28 GHz gyrotron. In the 28 GHz gyrotron project, a power output of over 1.5 MW has been achieved in the short pulse test, which is a new record in this frequency range [2].

In this paper, the empirical scaling of heat flux with P-ECH power is studied. In ECH power modulation experiments, new mirror antennas are used for controlling

author's e-mail: [minami@prc.tsukuba.ac.jp](mailto:minami@prc.tsukuba.ac.jp)

<sup>\*)</sup> This article is based on the presentation at the 12th International Conference on Open Magnetic Systems for Plasma Confinement (OS2018).

and generating higher intermittent heat flux in GAMMA 10/PDX. These findings can potentially be used for future divertor simulation studies.

## 2. Experimental Apparatus

Plasma experiments have been conducted in GAMMA 10, which is a minimum-B anchored tandem mirror with outboard axi-symmetric plug and barrier cells, as shown in Fig. 1.

Plasma confinement is achieved by a magnetic mirror configuration as well as positive and negative potentials at the plug/barrier region formed by ECH. The main plasma confined in the central cell of GAMMA 10 is produced by the ion cyclotron range of frequency wave. ECH systems (28 GHz, 200 kW at barrier cells, and 500 kW at plug and central cells) are prepared for producing plasma-confining potentials in the plug and barrier regions [3] and for direct electron heating in the central cell.

The flux and energy spectrum of the end-loss electrons are measured using a multi-grid energy analyzer (loss electron diagnostics, LED), as shown in Fig. 2. End-loss electrons enter the analyzer through a small hole on an electrically floating end plate located in front of the end wall. The collector current of the analyzer corresponds to the electron current flowing into the end plate. Using the LED analyzer, the energy-loss distribution of the particles reaches  $\sim 10$  keV. The energy selection is made by the negatively biased electron repeller grid in front of the collector, which is connected to the machine ground through a low resistance to measure the electron current. The biasing voltage ( $-V_{ER}$ ) of the electron repeller grid is swept during a shot. The LED is located at  $r = 30$  cm behind the innermost end plate and is connected to the magnetic field line that runs 2.8 cm off the axis at the 1 T layer in the plug region.

The ion currents are measured with spectrometer ar-

rays for end-loss ion energy analyses. Each spectrometer unit in the array has a specific structure with obliquely placed multiple grids with respect to the direction of the ambient plasma-confining magnetic fields. This structure enables a precise ion energy spectrum to be obtained without disturbance from incident energetic electrons, ranging from a few to several tens of keV, into the array [4].

The radial profile of the heat flux density is measured using a movable calorimeter. This diagnostics instrument is located 30-cm downstream from the end-mirror coil ( $z_{EXIT} = 30$  cm) and can be inserted from the bottom of the vacuum vessel up to the center axis of GAMMA 10. This instrument is also capable of rotating around the shaft, which allows measuring the direction of the plasma flow to the magnetic field line. The radial profile of heat flux at  $z_{EXIT} = 30$  cm can be obtained by changing the radial position [5].

The P-ECH system and location of the diagnostic systems used in the preliminary P-ECH modulation experiment to generate the high and ELM-like heat flux are shown in Fig. 1. In the vacuum vessel, a launcher composed of an open ended corrugated waveguide and two mirrors (M1 and M2) is installed. The launcher radiates the microwave power to the resonance layer, as shown in Fig. 1. The microwave beam is obliquely injected into the resonance surface at  $54^\circ$ . The mirror M2 can be rotated around the horizontal axis and can change the beam direction.

To generate higher heat flux, a high efficiency mirror antenna must be designed. The mirror design determines the surfaces of M1 and M2. The shapes of M1 and M2 are represented using analytical functions that include several parameters. Figures 3 (a) and 3 (b) show the calculated power density profiles on the resonance layer obtained for the previous mirror (M1) and new mirror (M2) designs. In the new design, the e-folding radius,  $w$ , of the radiation distribution power density on the resonance surface is 40 mm

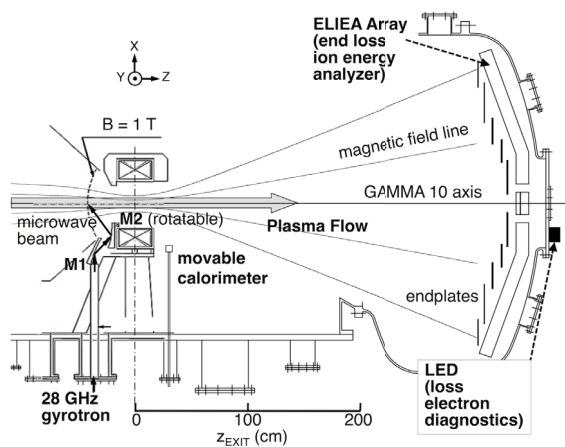


Fig. 1 Cross section of a plug/barrier and end regions in the GAMMA 10 tandem mirror. Microwave power is injected into the 1.0-T surface from the antenna. An LED analyzer is installed behind the innermost endplate.

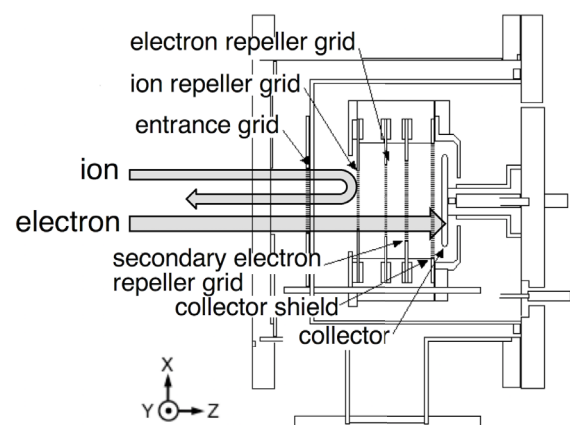


Fig. 2 Schematic of a multi-grid energy analyzer (loss electron diagnostics, LED).

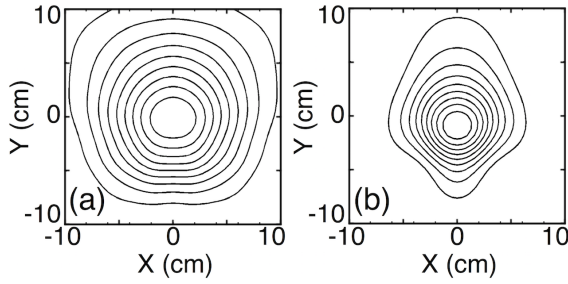


Fig. 3 Power density profiles of the resonance surface radiated from (a) previous and (b) new mirror antennas, respectively. Each origin indicates the GAMMA 10 axis. The contours are linearly plotted and the outermost contour indicates one-tenth of the peak power density.

and only the M2 surface is arranged without changing the other mirror (M1). The power density on the axis is inversely proportional to the square of  $w$ . Thus, if the new mirror (M2) is applied to the ECH system, more than two-fold enhancement in the power density on the axis can be expected.

### 3. Experimental Results

#### 3.1 Control of end-loss plasma flux by plugging potential

The plasma experiment for the control of end-loss fluxes uses a plasma discharge after  $t = 50$  ms (Fig. 4). For only one side of the P-ECH (west side) at  $t = 200 - 210$  ms, an ECH power of  $\sim 380$  kW is applied (gray region between dot-lines in Fig. 4).

During P-ECH injection, a multi-gridded electrostatic energy spectrometer (LED) is used to measure an increase in the end-loss electron current (Fig. 4 (b)). The pulse train of the electron current is due to the repeller voltage sweeping for energy analysis. Its envelope represents the electron current. Similarly, the end-loss ion current increases during P-ECH injection (Fig. 4 (a)) and its envelope represents the ion current. Thus, ion and electron fluxes are increased simultaneously and are controllable by one-sided P-ECH power modulation.

The P-ECH can modulate electrons by driving the two types of velocity space diffusions. The first type of diffusion enhances mirror reflection beyond the plug position, which results in the plug potential. On applying ECH to one side of the plug region, the opposite side of the end-loss ion current increases owing to the potential reflection of low-energy ions (Fig. 4 (a)). The second type of diffusion creates the electron flow (Fig. 4 (b)). These data indicate that the P-ECH can control the end-loss ion and electron fluxes via power modulation, which can also produce the arbitrary heat load pattern, similar to the various types of ELMs.

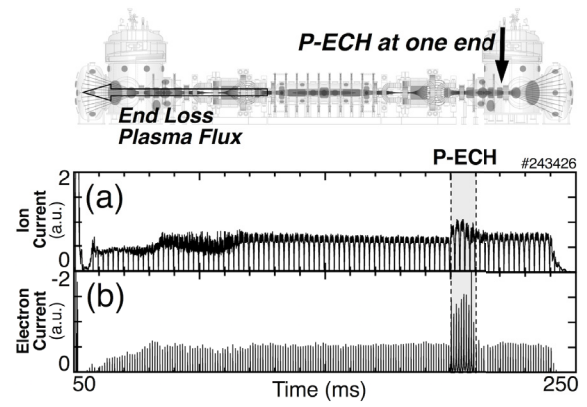


Fig. 4 Temporal evolution of (a) end-loss ion current and (b) end-loss electron current at the east end. The P-ECH power of approximately 380 kW at the west side region is applied at  $t = 200 - 210$  ms. Their envelopes represent ion and electron currents, respectively.

#### 3.2 Generation of high energy electron flux

Next, the plasma experiment for generating high-energy end-loss electron flux is conducted using high-power P-ECH, which is applied at the side regions of the P-ECH systems.

The flux,  $I_e$ , flowing into the collector of the LED is plotted as a function of the electron repeller voltage,  $V_{ER}$ . Both the flux and the mean energy increase with increasing P-ECH power,  $P_{P-ECH}$ . The energy spectra of the end-loss electrons cannot be expressed using a single component Maxwellian; however, they are well-fitted to a two-component Maxwellian as follows:

$$I_e = I_L \exp\left(-\frac{V_{ER} + \Phi_{EP}}{T_{eL}}\right) + I_H \exp\left(-\frac{V_{ER} + \Phi_{EP}}{T_{eH}}\right).$$

Here,  $\Phi_{EP}$  is the end-plate potential (for  $\Phi_{EP} < 0$ ).  $T_{eL}$  denotes the temperature of the bulk component, and  $T_{eH}$  denotes the temperature of the high-energy tail component.  $I_e$  is constant because the end plate effectively functions as an electron repeller. Using these parameters, an effective temperature,  $T_{eff}$ , is defined as the measure of the mean energy as follows:

$$T_{eff} = (1 - \beta)T_{eL} + \beta T_{eH},$$

where  $\beta$  is the flux fraction of the  $T_{eH}$  component to the total flux:  $\beta = I_H / (I_L + I_H)$ , where  $\beta$  is evaluated at  $V_{ER} = |\Phi_{EP}|$ . The typical energy distribution of electrons is plotted in Fig. 5 (a).

Preliminary experiments have been conducted to clarify the effects of the new mirror antenna (M2) with a narrower power density profile. In this experiment, the new mirror antennas have been applied to both sides of the P-ECH systems. Figure 5 (b) shows the power,  $P_e$ , of the electron end loss as a function of the P-ECH power,  $P_{P-ECH}$ . The axial heat flow is estimated from the product of effective electron temperature,  $T_{eff}$ , and electron current,

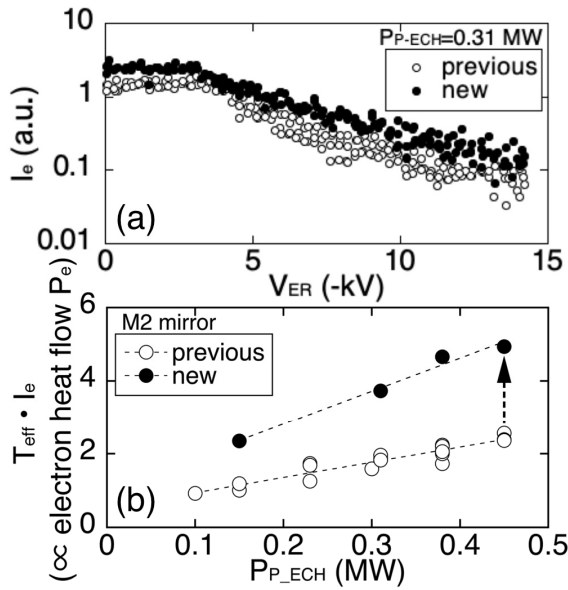


Fig. 5 (a) Energy spectra of the end-loss electrons measured using the LED analyzer for  $P_{P-ECH} = 0.31$  MW in previous (open circle) and new (closed circle) mirror antennas. (b) The end-loss electron power [value of the product of effective electron temperature,  $T_{eff}$ , and electron current,  $I_e$ ] is plotted as a function of the P-ECH power,  $P_{P-ECH}$ . These data are obtained using previous (open circle) and new (closed circle) mirror antennas.

$I_e$ , measured using the LED. Figure 5(b) shows that  $T_{eff}$  and  $I_e$  have increased due to the use of the new mirror antenna (M2).

Thus, concentrated power density can generate higher heat flux on the GAMMA 10 axis.

A difference in plasma parameters from calorimeter insertions has not been observed in this plasma experiment because the position of the calorimeter is changed shot by shot. Unfortunately, the heat flux density of the calorimeter and end-loss electron current of the LED cannot be measured simultaneously. The detailed electron properties are measured using the LED in the case of the off-axis calorimeter.

Using a movable calorimeter during the P-ECH injection, the peak heat flux can reach over  $30 \text{ MW/m}^2$  on the GAMMA 10 axis (Fig. 6). The heat flux continues to increase with increasing ECH power. This is one of the parameters that demonstrate the strong effects of the P-ECH. This value is still lower than the ITER level (mitigated ELMs in ITER is approximately  $0.5 \text{ MJ/m}^2$  for  $t = 0.5$  ms); however, it is expected to approach the ITER level by upgrading and combining all heating systems.

The heat flux continues to increase linearly with ECH power. Thus, the deposition power around the axis is presumably proportional to the power density of the P-ECH power on the axis. The power density on the axis is inversely proportional to the square of the e-folding radius,  $w$ . Thus, if the new mirror (M2) is applied to the ECH system, more than two-fold enhancement in the power density

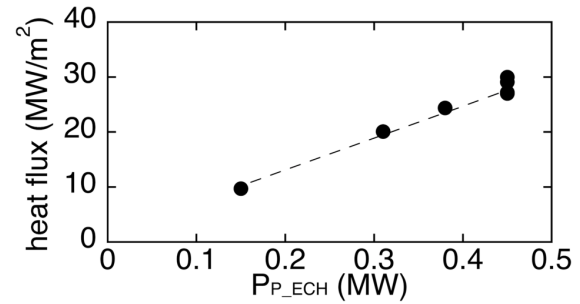


Fig. 6 The P-ECH power,  $P_{P-ECH}$ , is plotted as a function of heat flux at an axis position 30 cm from the mirror throat. A peak heat flux of over  $30 \text{ MW/m}^2$  is obtained.

on the axis can be expected. This estimation is based on the use of linear assumption, which roughly estimates the required gyrotron power.

Recently, a 28 GHz gyrotron achieving over 1.5 MW for GAMMA 10 and other low B field device ECH sources has been developed. Designing multi-MW and multi-frequency technologies is a major challenge for robust and cost effective reactor heating systems. GAMMA 10/PDX project has primarily focused on developing high-power 28 GHz gyrotrons. In the 28 GHz gyrotron project, an output power of  $>1.5$  MW has been achieved in the short pulse test, which is a new record in this frequency range. By upgrading the ECH system to the MW level, the effects of ELM-like repetitive pulsed heat loads on PFMs can be determined. Moreover, the ITER level heat flux factor can be obtained. The current maximum output of the new gyrotron is 1.65 MW [6]. Thus, if the new gyrotron is applied to the ECH system, two- to three-fold enhancement in ECH power sources can be expected. Future studies will be aimed at installing the new gyrotron for the west side P-ECH.

## 4. Summary

ECH power modulation experiments in GAMMA 10 have been conducted to generate and control the high heat flux for divertor simulation studies. This study analyzed the characteristic features of end-loss electrons using the LED electrostatic energy analyzer. The loss flux contains multiple components and is mostly composed of warm electrons with energies from several hundred eV to a few keV. Until now, the peak heat flux on the GAMMA 10 axis during P-ECH injection has reached  $30 \text{ MW/m}^2$  and continues to increase with applied ECH power. This significant increase in end-loss electron power is because of using improved mirror antennas. The effectiveness of concentrated power density has been confirmed for the generation of higher heat flux on the GAMMA 10 axis. Despite this advancement, achieving the ITER level ELM energy density will likely require an upgrade in the system and the combination of a multi-MW gyrotron and the new GAMMA 10 mirror antenna.

## Acknowledgments

The author thanks the members of the GAMMA 10 group of the University of Tsukuba for their collaboration and valuable discussion during this study. This work is partially supported by the grant-in-aid for Scientific Research from Ministry of Education, Science, Sports and Culture of Japan (26249141) and National Institute for Fusion Science (NIFS) Collaborative program (NIFS17KUGM126).

- [1] T. Imai *et al.*, *Trans. Fusion Sci. Tech.* **63**, 1T, 8 (2013).
- [2] T. Kariya *et al.*, *Nucl. Fusion* **57**, 066001 (2017).
- [3] K. Yatsu *et al.*, *Nucl. Fusion* **39**, 1707 (1999).
- [4] T. Kuwabara *et al.*, *Rev. Sci. Instrum.* **65**, 936 (1994).
- [5] Y. Nakashima *et al.*, 23rd IAEA Fusion Energy Conf. FTP/P1-33 (2010).
- [6] T. Kariya *et al.*, 27th IAEA Fusion Energy Conf. FIP/P1-56 (2018).